Internal and external modulation of folding rates with 10^4 to 10^5 year time resolutions from growth strata, Pico del Aguila, Spain

David J. Anastasio[1], Kenneth P. Kodama[1], Josep M. Parés[2], Linda A. Hinnov[3], Bruce D. Idleman[1]

[1]Lehigh University, Earth & Environmental Sciences, 1 W. Packer Ave., Bethlehem, PA, 18015-3001 USA

[2]Centro Nacional de Investigación sobre la Evolución Humana, Department of Geochronology and Geology, Paseo Sierra de Atapuerca 3, Burgos, 090002, Spain

[3]George Mason University, Department of Atmospheric, Oceanic, and Earth Science, Fairfax, VA, 22030 USA

Corresponding author: David Anastasio (dja2@lehigh.edu)

Key points:

- variable folding rates, between 5.5˚and 90˚± 19°/myr over 100s kyr time increments, characterize Pico del Aguila anticline, Spain
- deformation rates are modulated by both intrinsic processes and extrinsic processes

ABSTRACT

High-resolution cyclostratigraphy in growth strata are used to reconstruct unsteady folding rates at the regional-scale Pico del Aguila anticline, southern Pyrenees, to evaluate deformation modulation. Magnetic polarity stratigraphy was used to determine absolute time and to calibrate cyclostratigraphy-based anhysteretic remanent magnetization intensity variations to establish precessional frequencies in the growth strata record. Incremental tilting rates were calculated between selected horizons over ~5.24 myr of fold growth. Careful treatment of uncertainties enhances confidence that the results are meaningful and results show significant variability in folding rates over time. The acceleration phase of fold growth was variable, punctuated by a prolonged period of tectonic quiescence, and correlated to sedimentation changes in the wedge-top basin. Shallow-dipping bedding intrinsically modulated the initial rates of folding for the first 25˚ of limb tilt until 38.9 Ma. Then, halotectonics in the Paleogene Jaca Basin extrinsically modulated accelerating folding rates for the next 42˚ of folding, until ~37.5 Ma. Finally, forelimb-steepening leading to geometric strain hardening and blunted folding rates for the last 21˚ of fold tightening and causing a thrust fault to cut the anticline's core. Folding ended at Pico del Aguila ~35.9 Ma. Calculated folding rates varied between 0°± 5.5˚and 90˚± 19°/myr over 100s kyr time increments. Variations in the folding rate of the Pico del Aguila décollement anticline are attributed to both intrinsic modulation as a result of progressive bedding steepening during folding and extrinsic modulation as a result of variable deltaic sedimentation rates in the wedge-top basin.

Plain Language Summary

A high-resolution age model, with careful consideration to uncertainties, is used to reconstruct deformation rates at Pico del Aguila, Spain. The age model is recovered from sedimentary rocks that were deposited during deformation using magnetic methods. Deformation exceeded 5.24 million years with variable speed. Variations in deformation rate are attributed to both internal and external causes.

1 INTRODUCTION

Geometric interpretations and chronologic data suggest that deformation in orogens is unsteady at all timescales, from rates determined from GPS geodesy (10^{-1} yr), seismology (10^{0} to 10^{1} yr), paleoseismology (10^{2} to 10^{3} yr), magnetostratigraphy (10^{4} to 10^{6} yr), biostratigraphically (10^{5} to 10^{6} yr) or isotopically dated synsedimentary structures (10^{5} to 10^{6} yr) (e.g., Suppe et al., 1992; Gunderson et al., 2013). But what processes modulate this deformation rate unsteadiness? In this paper, we focus on the 10^{4} to 10^{6} year timescales of folding.

At these timescales, intrinsic drivers of the deformation rate might include such processes as strain partitioning (e.g., Bennett et al., 2004), fault growth and linkage (e.g., McCartney and Scholz, 2016), stress fluctuations (e.g., Gold et al., 2017), or strain hardening and softening resulting from changes in deformation mechanism or orientation of anisotropy (e.g., Donath 1962; Donath and Parker, 1964; Ramsay, 1967; Dolan et al., 2016). Extrinsic factors that might affect deformation rates, i.e., those things that affect the system boundary conditions, include such things as variable plate forcing (e.g., Holl and Anastasio, 1995), changes in surface loads affecting the stress state of faults (e.g., Hampel and Hetzel, 2005), pore pressure transience (e.g., Shaffer and Tobin, 2011; Gold et al., 2017), or synorogenic

sedimentation or erosion (e.g., Burbank et al., 2003).

The velocity and steadiness of deformation rates can provide clues to what modulates the tectonic processes. Since growth strata record the combined influence of deformation and deposition, deformation rates and incremental deformation geometry can be extracted from well-dated and geometrically well-characterized growth strata geometries. In this study, a high-resolution age model was recovered from marine and continental growth strata dated with magnetic polarity stratigraphy and rock magnetic-based cyclostratigraphy determined at the precessional timescale, i.e., ~20,000 yr for ~5.24 myr (Kodama et al., 2010). Fold geometry was determined by down-plunge projection of precision GPS locations, interpretation of fold growth strata from 1:5000 orthophotographs, and 1:5000 scale DEM analysis of growth strata geometry to get a rare glimpse into the variation in folding rates through time and to reveal changes in the processes that modulate deformation.

Pico del Aguila is a regional-scale décollement anticline with a thrust faulted core that developed in the hanging wall of the frontal (Guarga) thrust sheet, External Sierras, Pyrenees, Spain (**Fig. 1**). Folding developed above a mobile gypsiferous shale unit within the hundreds of meter thick Triassic Keuper facies that floors an ~1 km thick stiffer unit in pre-growth stratigraphy that is dominated by carbonate rocks of Cretaceous to Middle Eocene age (Puideàbregas, 1975). There are also carbonate units within the Keuper facies that are referred to as the Mushelkalk facies and which manifest themselves as a broken formation (Mey et al., 1968), which includes cellular dolomite (Anastasio, 1992). The westward prograding growth strata consist of marine, deltaic, and continental facies up to 1.34 km thick, which eventually buried the anticline. Bedding in the growth strata on the western limb

of the fold shallows from a near vertical dip in Late Eocene carbonates to horizontal bedding in the overlying Oligocene fluvial strata (**Fig. 1**). Most of the folding occurred during the Late Eocene Arguis Fm. deposition, a deltaic flysch unit characterized by mixed carbonate and siliciclastic sediment (Pudefàbregas, 1975; Castelltort et al., 2003). A latest Lutitian to early Priabonian age of the Arguis Fm. is supported by multispecies biostratigraphy (Canudo, 1990; Canudo et al., 1991) and magnetic polarity stratigraphy (Hogan, 1993; Pueyo et al., 2002; Kodama et al., 2010; Rodriguez-Pinto et al., 2012; **Fig. 1**).

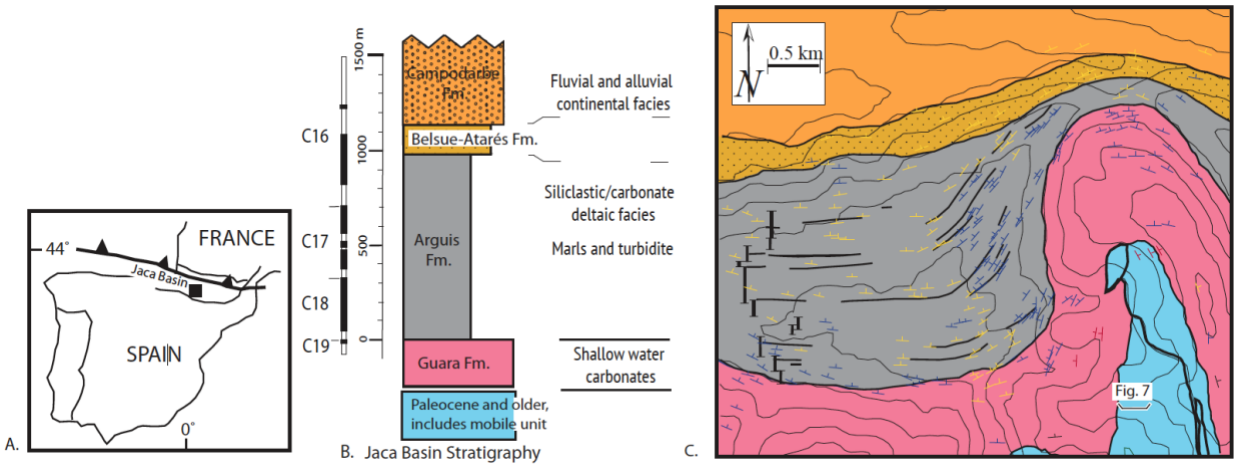

***Figure 1**. **A**. Index map showing Pico del Aguila (box) and the Jaca Basin in northern Spain. Pico del Aguila at solid square. **B.** Legend for stratigraphic units shown in **Figure 1C** and Jaca Basin magnetic polarity stratigraphy from Kodama et al. (2010), lithostratigraphy and environment of deposition. **C.** Geologic map of Pico del Aguila showing bedding measurements: shallow dip of bedding (<=30˚)-yellow, moderate dip (31˚-60)˚-blue and steep dip (61˚-90)˚-red. Stratigraphic section measured and samples for this study at the location of the bold black lines. UTM coordinates are shown at corners of the map.*

The train of External Sierras folds developed by differential loading halotectonics processes along the southern margin of the south Pyrenees wedge-top Jaca Basin (Anastasio,

1992; **Fig. 2**). This process of mobile strata migration in response to a prograding overburden is similar to the ongoing folding in the Gulf of Mexico (e.g. Bishop 1978; Ge et al., 1997). Pico del Aguila deformation overlapped in time with Guarga thrust sheet emplacement and wedge-top basin deposition (Anastasio, 1992).

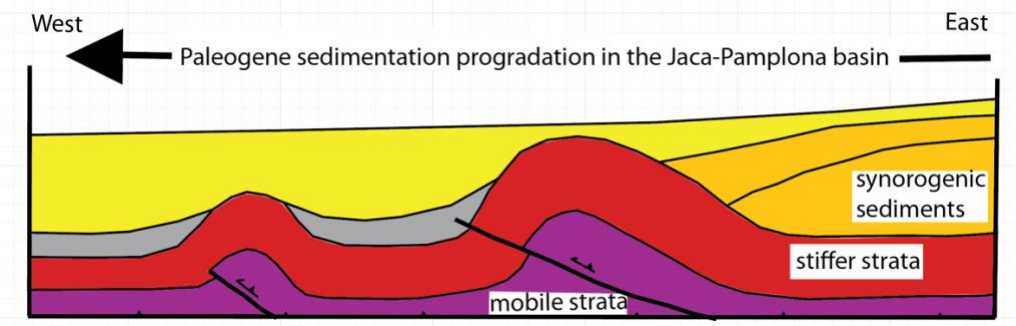

Figure 2*. Sketch of differential loading halotectonics, with transverse folding in the hanging wall of the schematic Guarga thrust sheet resulting from progradation of Paleogene synorogenic sediments in the Pyrenean wedge-top basin. Transverse folds develop in response to the prograding overburden.*

There have been many previous studies at Pico del Aguila anticline, including Puidefàbregas (1975), who mapped the Jaca Basin and studied the sedimentology of the Arguis Fm., Casselltort et al. (2003), who studied the stratigraphy of the growth strata around the anticline, Hogan and Burbank (1996), who reconstructed geohistory from the area's first magnetic polarity stratigraphy studies, Kodama et al. (2010), who used magnetic polarity stratigraphy and cyclostratigraphy to determine the detailed age of the growth strata horizons, Poblet and Hardy (1995), who analyzed growth strata geometries, and analogue and numerical modeling of the fold growth by Vidal-Royo et al. (2012; 2013). Pico del Aguila is a well-known synsedimentary

120 structure, where high sedimentation-to-uplift rates provides growth strata that records folding
121 in high fidelity.

122 **2 METHODS AND RESULTS**

123 **2.1 Fold Geometry**

124 Pico del Aguila is a tight, asymmetric, westward overturned, moderately north plunging,
125 décollement anticline in the central External Sierras (e.g., Anastasio et al., 2015). The folding
126 developed in the shallow crust, at <3 km of depth (Hogan and Burbank 1996) and <60˚C
127 (Anastasio and Holl, 2001). The fold geometry and fold orientation were determined during
128 field mapping as bedding data and formation contacts were collected (Anastasio, 1987). **Figure**
129 **3** shows that sedimentation accumulation rates increased during folding and that Pico del
130 Aguila was eventually buried by deltaic sediments (**Fig. 4**). The growth strata were mapped with
131 precision GPS using a local base station (cm scale accuracy), or with a handheld GPS with
132 barometric altimetry for elevation (m scale accuracy). To determine folding rates we also
133 interpreted growth strata on registered 1:5000 orthophotographs, on 1:5000 digital, 10m
134 elevation models, and took advantage of multiple measured sections (e.g. Puidefàbregas, 1975;
135 Castelltort et al., 2003; this study) with uncertainty on bedding thickness determined by Jacob
136 staff or tape measure conservatively estimated at ±5 m (1σ). Bedding locations, bedding
137 inclinations, and growth strata strike-lines were projected onto a dipping plane perpendicular
138 to the great circle defined by the average bedding orientations about the Pico del Aguila fold

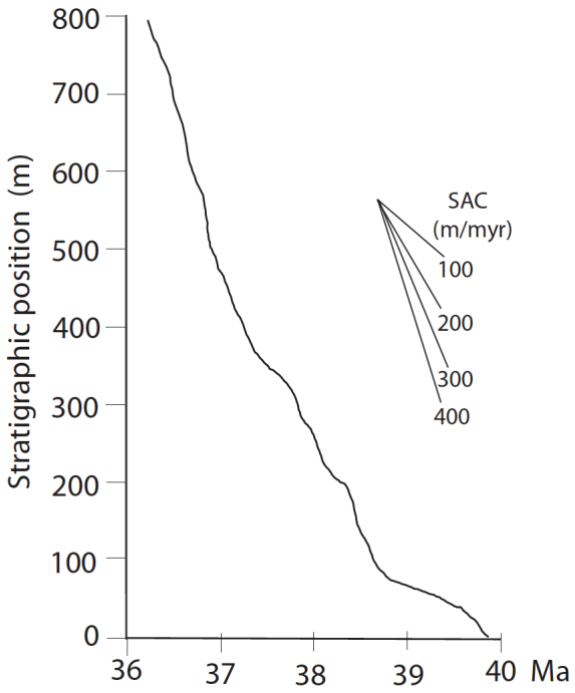

Figure 3*. Calibrated cyclostratigraphic age model of the stratigraphic column shown in* ***Figure 1B.*** *The age model is based on La2004 precession index tuning of the ARM time series (Fig. 5.5 in Kodama and Hinnov, 2014). Stratigraphic horizon ages were determined from the astrochronology, except first and last increments of folding where subchron averaged sedimentation rates were used to calculate the age model. SAC abbreviates sediment accumulation rate and line slopes show various SACs.*

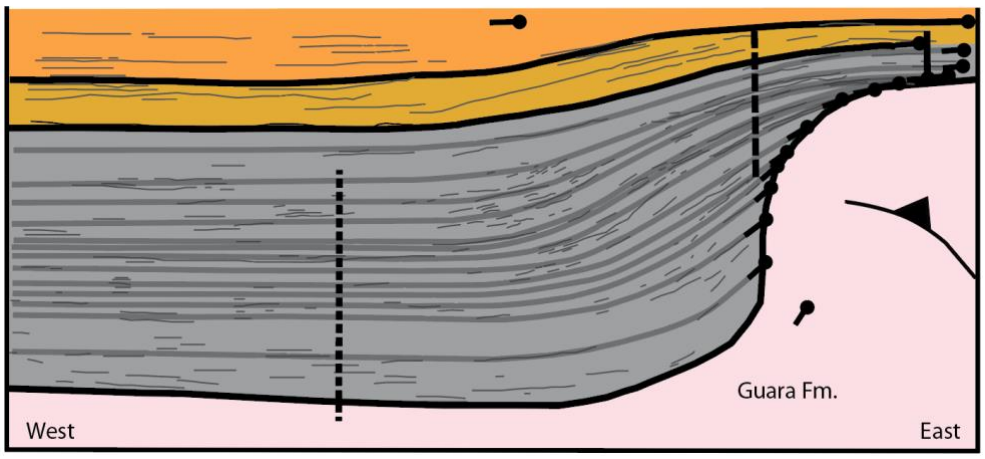

Figure 4. *Down-plunge projection of Pico del Aguila anticline drawn perpendicular to the great circle (profile plane) defining the fold. The orientation of the projected plane strikes 090˚ and*

dips 67˚S. Measured section locations at positions shown by vertical lines–shortest dash this study, longer dashed line Castellort, 2003, and solid line from Puidefàbregas, 1975 and Castelltort, 2003. Stratigraphy colors as in ***Figure 1****.*

(perpendicular to the fold axis). Mesoscopic faulting studies in pre-growth Guara limestones (Anastasio and Holl, 2001) and studies of growth strata geometry and their penetrative fabric (Anastasio et al., 2015) show that the Pico del Aguila anticline developed with fixed limb lengths and limb shearing towards a pinned fold hinge. The rotation of the fold limbs is also recorded by growth strata, which thin stratigraphically towards the anticlinal crest and shallow in dip, up-section. Incremental folding rates were determined for the west dipping limb of the fold in 14 time increments using the cyclostratigraphy results from Kodama et al., (2010) and magnetic stratigraphy results from Hogan and Burbank (1996), Kodama et al., (2010), and Rodrigiez-Pintó et al., (2012).

2.2 Growth Strata Chronology

Growth strata cyclostratigraphy was established in the Arguis syncline for a measured and sampled section located and dated in detail (**Fig. 1)**. From oldest to youngest, the growth stratigraphy of the External Sierras consists of shallow water carbonates at the top of the Guara Fm., marls and turbidites of the Arguis Fm., siliciclastic and carbonate deltaic facies of the Belsue-Atarés Fm., and the fluvial continental facies of the Campodarbe Fm. (**Fig. 1B**). Most of the folding at Pico del Aguila formed during the deposition of the Arguis Fm., the focus of our chronologic investigations. There was a gradual increase in the sediment coarseness and accumulation rates associated with delta progradation over top of the Pico del Aguila anticline (**Figs. 3** and **4**; Kodama et al., 2010). The growth strata record uplift exceeding sediment

accumulation early during folding leading to the onlap of growth horizons and sediment accumulation exceeding uplift at the end of folding leading to the growth strata burring the fold (**Figs. 1** and **4**).

Magnetic polarity stratigraphy and rock magnetic-based cyclostratigraphy were used to go from the stratigraphic depth domain to the time domain in the growth strata. A local paleomagnetic stratigraphy was correlated to the Geomagnetic Polarity Time Scale (GPTS; Gradstein et al., 2012) using existing biostratigraphy to establish absolute dates, assuming polarity reversals were at the midpoint between sampling sites of opposite polarity. Magnetic polarity reversals were then used to calibrate the anhysteretic remanent magnetization (ARM) data series which was used as proxy for magnetite concentration variations in the measured section. With a specimen analyzed every 3 kyr (nearly 1400 samples spaced 0.25-1.5m) and a specimen size which only integrates sediment accumulation over a few centuries, the ARM data series recovery of the cyclostratigraphy was robust. The detailed chronology of the growth strata was presented in Kodama et al., (2010).

2.3 Folding Rate Uncertainties

On a scale of 10^4 to 10^6 yrs, folding was variable and unsteady through time (**Fig. 5**). This conclusion includes a careful consideration of input uncertainties. In order to more easily handle the various calculation methods needed to determine folding rates in different parts of the section, the uncertainties were assessed using a Monte Carlo simulation. Uncertainties in bedding measurement locations and bedding pole orientations were estimated to be ±1° by down-plunge assessment or ±1.5° by repeated measurements with a geologic compass (uncertainties quoted at the 1σ). Errors on the stratigraphic position of strike lines ranged from

194 ± 5 - 25 m, depending on the depth in the growth section. Relative uncertainties in magnetic
195 chron ages were assumed to be ± 20 kyr, and uncertainties in chron positions within the section
196 were based on the paleomagnetic site spacing (3 m) that was determined by Jacob staff and
197 compass (**Fig. 5**). For the purposes of the Monte Carlo model, the stratigraphic positions of
198 paleomagnetic chron boundaries were allowed to vary with uniform weight over the full extent
199 of the sample spacing, whereas other uncertainties were assumed to be normally distributed.
200 Within the astronomically tuned portion of the section, depositional ages were determined by a
201 look up function for sediment accumulation rates determined by the cyclostratigraphy and
202 previously published in Kodama et al., (2010) (Fig. 9 in Kodama et al., 2010; **Fig 3**). Uncertainty
203 in relative time in this part of the section is estimated to be ±10,000 years (half a precessional
204 cycle), since the section was tuned at the precessional scale (Fig. 5.5 in Kodama and Hinnov,
205 2014). The model runs typically converged to better than 1% relative uncertainty in <100
206 iterations, but all of our quoted folding rate uncertainties are based on runs of 1000 iterations.
207 Site spatial errors and the correlation of the proxy ARM record to seasonal variations in
208 insolation are correlated and therefore were not propagated. Small but correlated errors due to
209 sample sizes (< few centuries) and orbital motions were also not propagated. All reported
210 astronomical ages include a ±2.5 kyr error due to uncertainty in the season of insolation forcing.
211 Additional timing errors also played into the modeling uncertainties in some cases: the ages
212 used are likely 1 kyr too old due to application of the La1993 astronomical target (Laskar et al.,
213 1993) in Messinian tuning (e.g., Hilgen et al., 2007) compared with those of the La2004 target
214 (Laskar et al., 2004), and up to 2 kyr too old due to uncertainties in tidal dissipation (Lourens et
215 al., 2004). The beginning and end phases of folding were determined by bedding dip and

magnetic polarity stratigraphy, only (**Fig. 5**). During these increments the age errors were also assigned to be ±10,000 yrs. Bedding inclination uncertainty was surprisingly the largest source of error in the folding rate calculations. This uncertainty is attributed primarily to bedding surface irregularities in the stratigraphic facies investigated, rather than to issues with the measurement process itself.

Overall, the limb tilt increased to a maximum and decreased abruptly as bedding steepened and Pico del Aguila became buried (**Figs. 1** and **5**). Calculated folding rates varied between 0˚±5.5˚ and 90˚±19 ˚/myr over 100's kyr time increments and were in pace with sedimentation rates. The fastest tilting rates occurred when bedding was at modest inclinations and formation strength was lowest as predicted by flexural-slip folding kinematics with mechanically-active bedding planes (**Fig 6**). Overall, sediment accumulation rates varied over two orders of magnitude between <0.1m/kyr and >1m/kyr (**Fig. 5**).

3 DISCUSSION

Empirical results from this high-resolution study confirms some expectations of folding but contradict others. Examination of **figure 5** shows that when chronologic resolution is only by biostratigraphy or magnetic polarity stratigraphy, such as at the beginning and end of the folding, the time resolution relative to cyclostratigraphy is degraded (e.g., Gunderson et al., 2015). The uncertainty analysis shows that the folding rate in a deltaic sequence is most sensitive to the bedding inclination change and time resolution between the assessments. As predicted by buckling theory, a folding instability (e.g., Sherwin and Chapple, 1968) occurred as a result of upstream delta progradation inducing E-W compression in the External Sierras (Anastasio, 1992). Following the onset of folding, the folding rate increased more than five-fold

before slowing rapidly and finally ending ~5.24 myr after folding began.

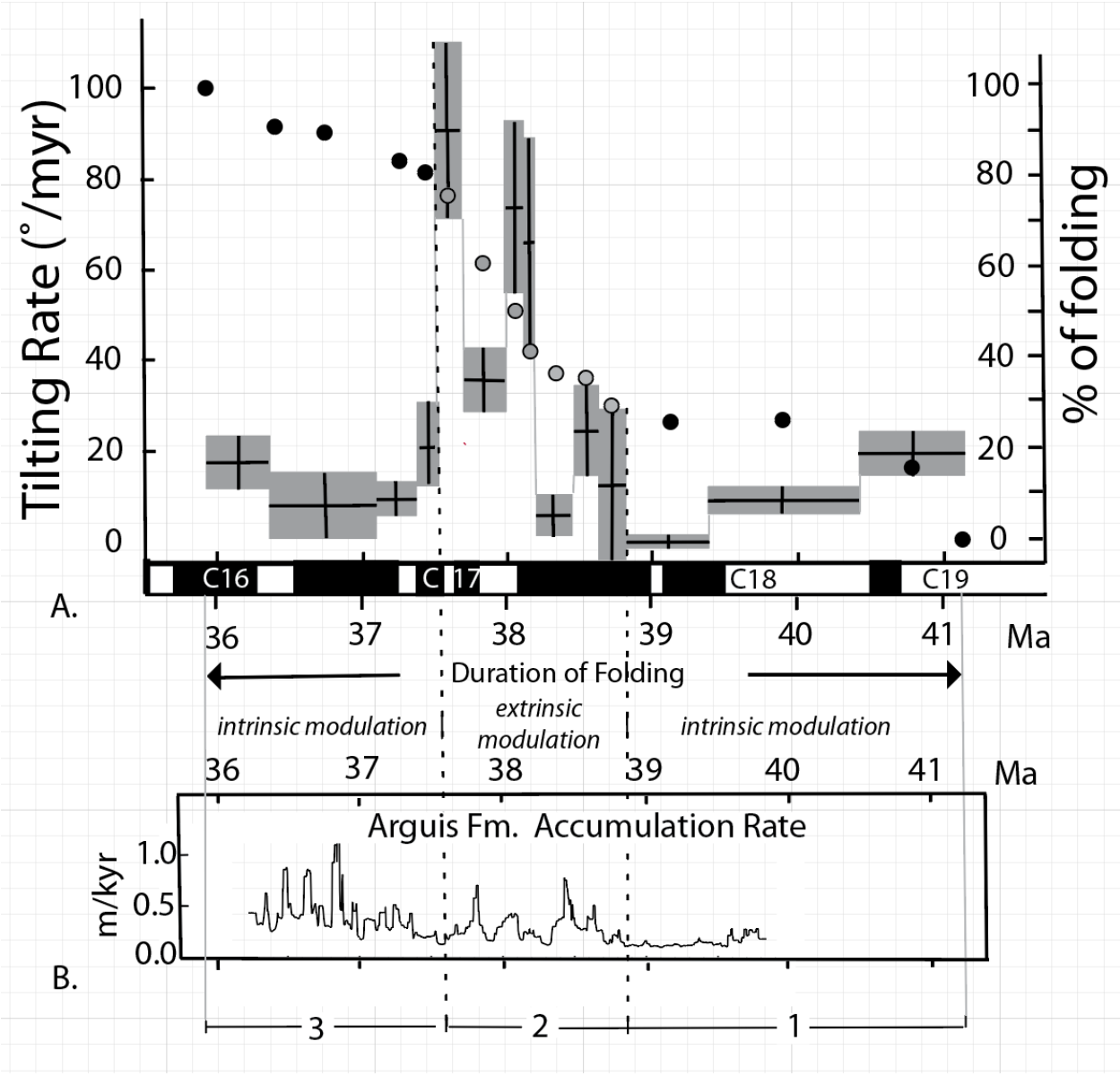

Figure 5. *Incremental fold rate assessment. West limb of Pico del Aguila tilting rate through time.* ***A****. Each increment of folding is indicated by a box size equivalent to uncertainties in folding rate and age. The errors in absolute age of the beginning and ending increments of folding are assigned to be 10,000 years, according to the astrochronology constrained increments, but ages are based on magnetic reversal chronology only. The second y-axis shows*

the percent of tilting. The grey and black dot colors are maintained in ***Figure 6*** *with times indicated by the grey dots representing extrinsic modulation of folding amounts and black dots indicating times of intrinsic modulation'* ***Figure 5B*** *shows the sediment accumulation rate determined from the tuned ARM time series of Kodama and Hinnov (2014). The duration of folding is a indicated by the double-headed arrow. Correlation of accumulation rates and folding amounts documents the extrinsic modulation of folding rates.* ***1****. Time of initial intrinsic modulation, including a time of condensed sediment accumulation and no folding.* ***2****. Time period of rapid folding and extrinsic folding modulation* ***3****. Intrinsic modulation because of bedding orientation corresponding to the period of fold burial.*

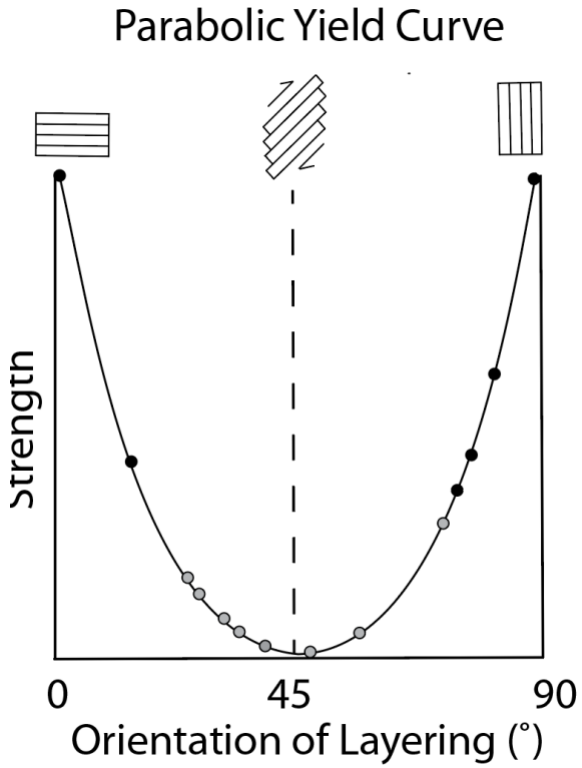

Figure 6. *Parabolic yield curve showing the same amounts of folding as in* ***Figure 5.*** *The strength is relative, and the figure shows the early and late periods of intrinsically modulated folding when layer orientation is expected to result in higher strength and the period of extrinsically modulated folding as a result of sedimentation variations.*

Studies of stress during orogenesis reconstruct values that vary with measurement technique and position within the orogen (e.g., Newman, 1994; Holl and Anastasio, 1995). Holl and Anastasio (1993) report westward progradation of fluvial environments within the transported wedge-top basin delta at 500 m/myr between 51 Ma and 43 Ma at Mediaño anticline, nearly 50 km to the northeast of Pico del Aguila and Holl and Anastasio (1995) report a reorientation of the principal shortening directions to E-W in the vicinity of the Boltaña lateral ramp ~30 km northeast of Pico del Aguila.

Based on folding theory, the explosive amplification of the folding rate is predictable (e.g., Hudelston, 1973). More surprising is the cessation of folding for >0.5 myr, well after folding began and before further folding again commenced at increased rates before slowing to conclusion (**Fig. 5**). A pause in deformation was also observed by Carrigan et al. (2018) for a fault-propagation fold further east in the Pyrenees that the authors attributed to a pause in thrusting in the studied fault-related fold. The cessation of folding correlates in time with a period of slow synorogenic sedimentation, resulting in a condensed growth section as a result of little sediment loading. At the base of the Arguis Fm. neritic facies with abundant glauconitic strata attests to frequent diastems and slow sedimentation.

Shear strain between mechanical layers, however, is the critical variable for flexural folding in layered rocks (e.g. Ramsey, 1967). An upward convex parabolic yield curve predicts the folding rate curve for flexural folds with shear on bedding planes (the main surface of weak anisotropy; **Fig. 6**). The attitude of horizontal bedding makes it more difficult to initiate folding. Then as bedding rotates, it geometrically strain softens, minimizing the incremental stress and strain required for further tilting as bedding rotates to moderate angles. As bedding continues

to steepen further folding becomes harder again (e.g., Donath, 1962; Fisher, 1990), and at tight interlimb angles, folds lock-up due to geometric strain hardening. For example, at the Pico del Aguila anticline, the folding rate diminished greatly in the Late Eocene when the interlimb angle reached 55˚ and stopped altogether by the Early Oligocene, even though shortening in the External Sierras continued until the Early Miocene (Anastasio, 1992).

3.1 What Controlled The Rate Of Folding At Pico Del Aguila Anticline?

Folding in the External Sierra gets progressively younger and the folding is of smaller amplitude further west in the range, consistent with folding caused by differential loading halotectonics (e.g. Anastasio, 1992; **Fig. 2**). Folding ceased when synorogenic sedimentation was very slow and increased in a pulsating fashion as deltaic sedimentation rates varied (**Fig. 5**). Coarsely gridded climate models by Sloan and Huber (2001) showed up to 15% variability in river runoff at precessional frequencies in the strike parallel river feeding the wedge-top delta. For the 2 myr, between 39.5 Ma and 37.5 Ma, the sediment accumulation rates around Pico del Aguila varied with orbital forcing (**Fig. 5**). This is also the time period when limb tilting is variable, beating in time with sedimentation rate. This time corresponds with modest bedding inclination and cyclic sedimentary accumulation rates supporting the differential loading hypothesis and the conclusion of extrinsic modulation of folding. Exposures of the incompetent Triassic Pont de Suert Fm. (includes the Keuper facies evaporites and shales) in the Pico del Aguila anticlinal core are everywhere deformed and the formation varies in thickness from 0 m in synclinal salt welds to >2 km beneath the anticlines where the flowage of the Keuper facies was greatest. What remains unclear is to what degree the incompetent Triassic Keuper facies that cores the fold played in the transition from external to internal modulation. In models of

halotectonic folding driven by progradation, growing anticlines only continue to amplify while the adjacent salt is deflating below the prograding sediment wedge (Ge et al., 1997). Once the entirety of the mobile unit has been removed from the prograding wedge, the adjacent fold no longer grows by amplification, but would simply migrate in front of the prograding sediments. This conceptual model is consistent with the 3D restoration of Pico del Aguila by Vidal-Royo et al., (2012), which indicated a late-stage switch from fold amplification to fold migration as evidenced by the migration of the synclinal hinges.

Thrust faulting in the core of the Pico del Aguila décollement anticline breached the lower Guara Fm. after fold tightening (e.g., Gonzalez-Mieres and Suppe, 2006; **Fig. 7**).

Figure 7. *Field photograph of the core of Pico del Aguila, looking north. Late thrust fault decapitating anticline in fold's core to accommodate fold tightening. Photograph view shown in* ***Figure 1C.***

The pause in folding after initiation is recorded by constant dip and parallel beds in the growth strata (**Fig. 4**). Climate cycles were expected to have caused both runoff variation in the southern Pyrenees Paleogene rivers (e.g. Sloan and Huber, 2001) and variation in sedimentary facies and progradation rates during the pause in folding at Pico del Aguila. The buried geometry of Pico del Aguila is ridge-like to the north beneath the Jaca Basin. It is unlikely, that river avulsion within the Paleogene delta and the resulting change in the locus of deposition

could have affected the variations in folding rate and river avulsion in deltaic environments is likely to occur at a much faster rate than precessional frequencies, ranging from decades to millennia (e.g. Hajek and Wolinsky 2012; Foreman and Straub, 2017), therefore, this processes too, is unlikely to explain the folding rate behavior.

Initially (at 41.2 Ma - 38.9 Ma), folding rates were intrinsically controlled by shallow bedding orientation. Following this initial stage, variations in boundary conditions began to occur along the synorogenic surface. Here, climate affected runoff variation in the wedge-top basin strike-parallel river, which in turn, controlled the deltaic sedimentation accumulation rates around Pico del Aguila, the ultimate cause of the differential loading halotectonics. After 37.6 Ma, fold tightening led to geometric strain hardening and a slowing of folding rates (**Fig. 5**). This was again, a time period of intrinsic fold modulation. The strain hardening then led to late-stage contractional faulting in the fold's core. Gunderson et al. (2018) found similar evidence of intrinsic modulation of deformation at 10^4 to 10^5 yr timescales in a study of thrusting rates done in the central Apennines, Italy.

4 CONCLUSIONS

Using a high-resolution chronology of the growth strata surrounding Pico del Aguila anticline, incremental folding rates were reconstructed for the buried fold. Folding at Pico del Aguila occurred over an ~5.24 myr period at unsteady rates at 10^4 and 10^5 yr timescales. Monte Carlo analysis of folding rate uncertainties, including spatial positions, bedding orientations, growth strata geometries, chron boundary ages, and paleomagnetic site spacing, demonstrate statistically significant variations in folding rates at the anticline. Folding rates varied between 0˚±5.5˚/myr and 90˚±19˚/myr. Folding temporarily ceased in the Late Eocene, then accelerated

346 to a maximum rate, and then decelerated once again toward the end of folding. Initially, folding
347 rates were controlled by intrinsic factors related to the shallow dip of bedding. Subsequent
348 variable folding rates are attributed to episodic sediment accumulation in the axial wedge-top
349 basin, an extrinsic modulation. Sediment accumulation rates increased as the delta prograded,
350 then folding rates began to respond to intrinsic modulation related to the steepening of Guara
351 Fm. bedding, with slower folding rates and late-stage thrust faulting occurring within the fold's
352 core.

353 **ACKNOWLEDGMENTS**

354 Field and laboratory research were assisted by Michael Newton and Christine Regalla,
355 Lehigh University and Jim Greenberg, UNAVCO, Inc. Research funding was provided by NSF EAR-
356 0409077. No authors have any real or perceived financial or affiliation conflicts of interest. Data
357 supporting the chronologic model of the growth strata were first published in Kodama et al.,
358 2010. This paper was written while the first author was a Visiting Professor at Centro Nacional
359 de Investigación sobre La Evolución Humana (CENIEH), Burgos, Spain. Kellen Gunderson is
360 thanked for his review of this manuscript. Juliet Crider and David Oakley are thanked for their
361 reviews of a previous version of the manuscript.

362 **REFERENCES CITED**

363 Anastasio, D. J. (1987*) Thrusting, Halotectonics, and Sedimentation in the External Sierra,*
364 *Southern Pyrenees, Spain* (Doctoral dissertation), Baltimore, Johns Hopkins University.
365 Anastasio, D. J. (1992) Structural Evolution of the External Sierra, Spanish Pyrenees. In S. Mitra,
366 S. and Fisher, G.W. eds., *The Structural Geology of Fold and Thrust Belts*, pp. 239-251,
367 Baltimore, MD, Johns Hopkins University Press.

368 Anastasio, D. & Holl, J. (2001) Transverse fold evolution in the External Sierra, southern
369 Pyrenees, Spain, *Journal of Structural Geology*, 23, 379-392.
370 Anastasio, D. J., Parés, J.M., Kodama, K.P., & Troy, J., Pueyo, E.M. (2015) Synsedimentary
371 Deformation at Pico del Aguila, Spain, recovered from AMS Data. In Pueyo, E.L., Cifelli, F.,
372 Sussman, A.J., Oliva-Urcia, B., (Eds.), *Palaeomagnetism in Fold and Thrust Belts: New*
373 *Perspectives*. Geological Society of London, Special Volume 425.
374 https://doi.org/10.1144/SP425.8
375 Bennett, R. A., Friedrick, A. M., & Furlong, K. P. (2004) Codependent histories of the San
376 Andreas and San Jacinto fault zones from inversion of fault displacement rates*, Geology*, 32
377 (11), 961-964.
378 Bishop, R. S. (1978) Mechanism of emplacement of piercement diapirs, *American Association of*
379 *Petroleum Geologists Bulletin*, 62, 1561-1583.
380 Burbank, D. W., Blythe, A. E., Putkonen, J., Pratt-Sitaula, B., Gabet, E., Oskin, M., Barros, A., &
381 Ojha, T. P. (2003) Decoupling of erosion and precipitation in the Himalayas, *Nature*, 426,
382 652-655.
383 Canudo, J. I. (1990) *Los foraminiferos planctonicos del Paleoceno-Eocene del Prepirineo oscense*
384 *en el sector de Arguis* (Doctoral dissertation), Zaragoza, Spain, University of Zaragoza.
385 Canudo, J. I., J. Malagon, A. Melendez, H. Millan, E. Molina, & Navarro, J. J. (1991) Las
386 secuencias deposicionales del Eoceno medio y superior de las Sierras exteriors (Prepirineo
387 meridional aragones), *Geogaceta*, 9, 81–84.
388 Carrigan, J. H., Anastasio, D. J., Kodama, K. P., & Parés, J. M. (2016) Fault-related fold kinematics
389 recorded by terrestrial growth strata, Sant Llorenç de Morunys, Pyrenees Mountains, NE

Spain, *Journal of Structural Geology*, 91, 161-176. http://dx.doi.org/10.1016/j.jsg.2016.09.003

Castelltort, S., Guillocheau, F., Robin, C., Rouby, D., Nalpas, T., Lafont, F., & Eschard, R. (2003) Fold control on the stratigraphic record: a quantified sequence stratigraphic study of the Pico del Aguila anticline in the south-western Pyrenees (Spain), *Basin Research*, 15, 527-551.

Dolan, J. F., McAuliffe, L. J., Rhodes, E. J., McGill, S. F., & Zinke, R. (2016) Extreme multi-millennial slip rate variations on the Garlock fault, California: Strain super-cycles, potentially time-variable fault strength, and implications for system-level earthquake occurrence, *Earth and Planetary Science Letters*, 446, 123–136. https://doi.org/10.1016/j.epsl.2016.04.011

Donath, F.A. (1962) Role of layering in geologic deformation. *Transactions New York Academy of Sciences*, Series 2, 24, p. 236-249.

Donath, F. A. & Parker, R. B. (1964) Folds and folding, *Geological Society of America Bulletin*, 75, 45-62.

Fisher, D. M. (1990) Orientation history and rheology in slates, Kodiak and Afognak Islands, Alaska, *Journal of Structural Geology*, 12, 483-498, https://doi.org/10.1016/0191-8141(90)90036-X

Foreman, B. Z. & Straub, K. M. (2017) Autogenic geomorphic processes determine the resolution and fidelity of terrestrial paleoclimate records. *Science Advances*, 3, e1700683.

Ge, H., Jackson, M. P. A., & Vendeville, B. C. (1997) Kinematics and dynamics of salt tectonics driven by progradation, *American Association of Petroleum Geologists Bulletin*, 81, 398-423.

410 Gold, R. D., Cowgill, E., Arrowsmith, J. R., & Friedrich, A. M. (2017) Pulsed strain release on the
411 Altyn Tagh fault, northwest China, *Earth and Planetary Science Letters*, 459, 291-300,
412 https://doi.org/10.1016/j.epsl.2016.11.024
413 Gonzalez-Mieres, R. & Suppe, J. (2006) Relief and shortening in detachment folds, *Journal of*
414 *Structural Geology*, 28, 1785-1807.
415 Gradstein, F. M., Ogg, J. G. Schmitz, M. D., & Ogg, G. M. (2012) The Geologic Time Scale 2012,
416 First Edition. Elsevier B. V. https://doi.org/10.1016/C2011-1-08249-8
417 Gunderson, K. L., Anastasio, D. J., Pazzaglia, F. J., & Picotti, V. (2013) Fault slip rate variability on
418 10^4-10^5 yr timescales for the Salsomaggiore blind thrust fault, Northern Apennines, Italy,
419 *Tectonophysics*, 240, 356-365. https://dx.doi.org/10.1016/j.tecto.2013.09.01.
420 Gunderson, K. L., Pazzaglia, F. J., Picotti, V., Anastasio, D. A., Kodama, K. P., & Rittenour, T.,
421 2014. Unraveling tectonic and climatic controls on synorogenic growth strata (Northern
422 Apennines, Italy), *Geological Society of America Bulletin*, 126 (3-4), 532–552.
423 https://doi.org/10.1130/B30902.1
424 Gunderson, K. L., Anastasio, D. J., Pazzaglia, F. J., & Kodama, K. P. (2018) Intrinsically variable
425 blind thrust faulting, *Tectonics*, 37, 1454-1471.
426 Hajek, E. A. & Wolinsky, M. A. (2012) Simplified process modeling of river avulsion and alluvial
427 architecture: Connecting models and field data, *Sedimentary Geology*, 257, 1–30.
428 Hetzel, R. & Hampel, A. (2005) Slip rate variations on normal faults during glacial-interglacial
429 changes in surface loads, *Nature*, 435, 81-4. https://doi.org10.1038/nature03562.

Hilgen, F., Kuiper, K., Krijgsman, W., Snel, E., & van der Laan, E. (2007) Astronomical tuning as the basis for high resolution chronostratigraphy: the intricate history of the Messinian Salinity Crisis, *Stratigraphy*, 4, 231-238.

Hogan, P.J. (1991) *Geochronologic, tectonic, and stratigraphic evolution of the Southwest Pyrenean Foreland, Northern Spain* (Doctoral dissertation), Los Angeles, CA, University of Southern California.

Hogan, P. J. & Burbank, D. W. (1996) Evolution of the Jaca piggyback basin and emergence of the External Sierra, southern Pyrenees: In Friend, P.F., Dabrio, Cristino J., (Eds.), *Tertiary Basins of Spain: The stratigraphic Record of Crustal Kinematics*. p. 153-160, Cambridge England, Cambridge University Press.

Holl, J. E. & Anastasio, D. J. (1993) Paleomagnetically Derived Folding Rates, Southern Pyrenees, Spain, *Geology*, 13 (3), 271-274.

Holl, J. E. & Anastasio, D. J. (1995) Kinematics around a large-scale oblique ramp, southern Pyrenees, Spain, *Tectonics*, 14, 1368-1379.

Hudleston, P. J. 1973. Fold morphology and some geometrical implications of theories of fold development, *Tectonophysics*, 16, 1-46.

Kodama, K. P., Anastasio, D. J., Newton, M. L., Pares, J. M., & Hinnov, L. A. (2010) High-resolution rock magnetic cyclostratigraphy in an Eocene flysch, Spanish Pyrenees, *Geochemistry. Geophysics, Geosystems*, 11, 1-22, QOAA07, https://doi.org/10.1029/2010GC003069

Kodama, K. P. & Hinnov, L. A. (2014) *Rock Magnetic Cyclostratigraphy*. New York, NY, Wiley-Blackwell. https://doi.org/10.1002/9781118561294

452 Laskar, J., Joutel, F. & Boudin, F. (1993) Orbital, precessional, and insolation quantities for the
453 earth from -20 Myr to +10 Myr. *Astronomy and Astrophysics*, 270,522-533.
454 Laskar, J. P., Robutel, F. Joutel, M. Gastineau, A. C. M. Correia, & Levrard, B. (2004) A long term
455 numerical solution for the insolation quantities of the Earth, *Astronomy and Astrophysics*,
456 428, 261–285. https://doi.org/10.1051/0004-6361:20041335
457 Lourens, L., Hilgen, F., Laskar, J., Shackleton, N. J., & Wilson D. (2004) The Neogene Period. A
458 Geologic Time Scale 2004. https://doi.org/10.1017/CBO9780511536045.022
459 McCartney, T. & Scholz, C. A. (2016) A 1.3 million year record of synchronous faulting in the
460 hangingwall and border fault of a half-graben in the Malawi (Nyasa) Rift, *Journal of*
461 *Structural Geology*, 91, 114-129.
462 Mey, P. H. W.,Nagtegaal, P. J. C., Robert, K. J., & Hartvelt, J. A. A. (1968) Lithostratigraphic
463 subdivision of post-Hercynian deposits in the south central Pyrenees, Spain, *Leidsche*
464 *Geologische Mededelingen*, 41, 221-228.
465 Newman, J. (1994) The influence of grainsize and grainsize distribution methods for estimating
466 paleostresses from twinning in carbonates. Journal of Structural Geology, 16, 1598-1601.
467 Poblet, J. & Hardy, S. (1995) Reverse Modeling of Detachment Folds – Application to the Pico-
468 del-Aguila Anticline in the South Central Pyrenees (Spain), *Journal of Structural Geology*, 17,
469 1707-1710.
470 Puigdefàbregas, C. (1975) *La Sedimentation Molasica en la Cuenca de Jaca*. Monograph 104,
471 Jaca, Instituto de Estudios Pirenaicos.
472 Pueyo, E. L., Millán, H., & Pocoví, A. (2002) Rotation velocity of a thrust: a paleomagnetic
473 study in the External Sierras (Southern Pyrenees), *Sedimentary Geology*, 146, 191-

208.

Ramsey, J.G. (1967) Folding and Fracturing of Rocks. New York, NY, McGraw-Hill Book Company.

Rodriguez-Pintó, A., Pueyo, E. L., Sierra-Kiel, J, Sanso, J. M., Barnolas, A., & Pocoví, A. (2012) Lutition magnetostritigraphic calibration of larger forminifera zonation (SBZ) in the southern Pyrenees: The Isuela section, *Paleoecology, Paleoclimatology, Paleoecology*, 333, 107-120.

Sherwin, J. A. & Chapple, W. M. (1968) Wavelengths of single layer folds: a comparison between theory and observation, *American Journal of Science*, 266, 167-179.

Sloan, L. C. & Huber, M. (2001) Eocene oceanic responses to orbital forcing on precessional time scales, *Paleoceanography*, 16, 101–111, https://doi.org/10.1029/1999PA000491

Shaffer, D. M., Tobin, H. J. (2011) Hydrogeology and mechanics of subduction zone forearcs: Fluid flow and pore pressure, *Annual Review of Earth and Planetary Sciences*, 39, 157-186.

Suppe, J., Chou, G. T., & Hook, S. K. (1992) Rates of folding and faulting determined from growth strata. In, McClay, K.R. editor, *Thrust Tectonics*. p. 105-122, New York, NY, Springer, ISBN 978-94-011-3066-0

Vidal-Royo, O., Cardozo. N., Muñoz, J. A., Hardy, S., & Maerten, L. (2012) Multiple mechanisms driving detachment folding as deduced from 3D reconstruction and geomechanical restoration: the Pico del Aguila anticline (External Sierras, Southern Pyrenees), *Basin Research*, 24, 295-313, https://doi.org/10.1111/j.1365-2117.2011.00525

Vidal-Royo, O., Muñoz, J. A., Hardy, S., Koyi, H., & Cardozo. N. (2013) Structural evolution of Pico de Aguila anticline (External Sierras, southern Pyrenees) derived from sandbox, numerical and 3D structural modeling techniques, *Geologica Acta*, 11, 1-26.